

Light-controlled THz plasmonic time-varying media: momentum gaps, entangled plasmon pairs, and pulse induced time-reversal

Egor I. Kiselev,^{1,2} Yiming Pan,³ and Netanel H. Lindner^{1,2}

¹*Department of Physics, Technion, Haifa 3200003, Israel*

²*The Helen Diller Quantum Center, Technion, Haifa 3200003, Israel*

³*School of Physical Science and Technology and Center for Transformative Science, ShanghaiTech University, Shanghai 200031, China*

This letter establishes a Floquet engineering framework in which coherent high frequency light with a time dependent amplitude can be used to parametrically excite and amplify THz plasmons, mirror plasmonic wave packets in time, generate momentum-gapped plasmonic band structures, entangled plasmon pairs, and THz radiation in two dimensional Dirac systems. Our results show how low frequency plasmons can be coherently excited and manipulated without the need for THz light.

Introduction. Time varying media [1], discussed by Morgenthaler as early as 1958 [2], and by Holberg and Kunz in 1966 [3], have recently attracted a great deal of attention due to a variety of exotic effects and potential applications. Notable examples are time-varying mirrors [4], space-time crystals [5, 6], time-varying metasurfaces [7–9], temporal switching [10–12], amplified emission and lasing [13], photon pair generation [13, 14], nontrivial topological [15] and statistical properties [16], non-Hermiticity [17, 18], momentum-gapped (k-gapped) states, and unusual solitonic behavior [19]. Beyond photonics, time varying media have been realized in classical liquids [20] and acoustic media [21, 22].

Floquet engineering of quantum materials, on the other hand, is a powerful tool for the manipulation of band structures and for creating non-equilibrium correlated states in atomic, optical, and condensed matter physics [23–51]. A recent work suggested that Floquet engineering using high frequency drives enables control of low-energy collective modes of many body systems through Modulated Floquet Parametric Driving (MFPD) and leads to new correlated states [52]. Here, we demonstrate that an amplitude modulated optical Floquet drive can be used to create momentum gapped plasmonic time varying media – terahertz (THz) analogues of so called photonic time crystals (PTCs) [15]. Plasmonic time varying media can be used to create entangled plasmon pairs, amplify plasmons, as well as reverse their propagation in time. MFPD surpasses experimental difficulties associated with the excitation and manipulation of low frequency plasmons: A high frequency (eV-range) drive is used to engineer an effective band structure. Varying the drive’s amplitude in time then creates a medium with time dependent properties.

Compared to many other solid state Floquet engineering schemes, MFPD offers two major advantages: First, the Floquet drive couples to a resonant mode (the plasmon), which stores its energy over many oscillation cycles and thus amplifies its effects. Second, it operates in a regime with strongly suppressed photon absorption and heating (see Fig. 1).

While we focus on THz plasmons in this manuscript,

we note that the MFPD principle is very general, and could be employed to create time varying media with other kinds of collective modes and at different frequencies. The main limitation with respect to the frequency range is that the amplitude modulation, which is responsible for the time-varying properties, is significantly slower than the carrier frequency of the Floquet drive. Potentially, MFPD can be applied to magnons in ferro- and antiferromagnets, which span a range of frequencies between GHz and THz [53, 54]. Here similar effects could be mediated by the renormalization of the effective exchange constant by coherent light [55–57].

Our starting point are electrons in a two dimensional material. An effective quasi-energy band structure is induced by driving the electrons coherently with light of frequency Ω_F . The induced band structure depends on the amplitude of the driving signal. A subsequent periodic modulation of the drive amplitude with a frequency $2\omega_1 \ll \Omega_F$ results in a periodically changing Fermi velocity. The oscillation of the Fermi velocity parametrically couples to the soft plasmon modes of the two dimensional electron gas. This is the principle of MFPD, which is illustrated in Fig.1. In this letter, we will consider plasmons with low frequencies of a few THz [58]. The principle, however, can be applied more broadly, depending on material and driving parameters.

In the linear approximation, the Floquet-engineered dynamics of the plane wave plasmon modes $\delta\rho_{\mathbf{q}}$ is governed by the equation

$$\partial_t (1 + h \cos 2\omega_1 t) \partial_t \delta\rho_{\mathbf{q}} + \omega_{\text{pl}}^2(q) \delta\rho_{\mathbf{q}} = 0, \quad (1)$$

which is derived below. Here h is an amplitude describing the effect of a slow modulation of the driving field (see Eq. (3)), and $\omega_{\text{pl}}(q)$ is the plasmon dispersion defined in Eq. (5). Equation (1) is a plasmonic version of the equation describing the evolution of electromagnetic waves in PTCs [13], where the driving enters through a modulation of the dielectric constant $\varepsilon(t)$.

In essence, Eq. (1) is a parametric oscillator equation describing parametrically excited plasmonic plane-wave modes. We note that momentum conservation requires that modes with wavevectors \mathbf{q} and $-\mathbf{q}$ are equally ex-

cited, such that the net momentum is zero [52]. Parametric resonance occurs for $\omega_{\text{pl}}(q) \approx n\omega_1$, with $n = 1, 2, 3, \dots$ (see Ref. [59] § 27). In the presence of damping, resonance occurs above a critical amplitude h_c , which grows with increasing n [60]. We will focus on the $n = 1$ case, which requires the lowest h_c . It can be useful to exploit resonances with $n > 1$ to lower the required modulation frequency [61, 62], however modulation frequencies of up to 10 THz can be reached by interfering laser beams with slightly detuned frequencies [63, 64].

This reveals another basic functionality of MFPD. It can be used as a frequency mixer, which creates standing wave plasmons at frequencies corresponding to the beating of the high frequency signal (see Fig. 1c)). These plasmons, which will have μm -wavelengths and create strong electric fields in the THz range (see the discussion of experimental parameters at the end of this letter), can be detected by near field optical microscopy [65, 66].

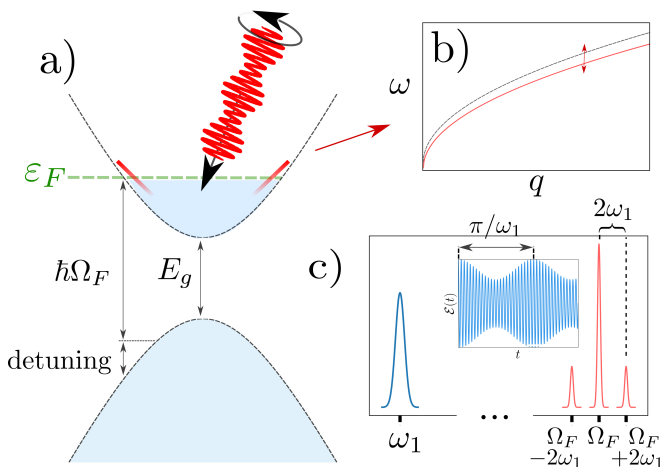


Figure 1. Floquet engineering and MFPD. a) The band structure (grey) of a gapped Dirac material, e.g. a transition metal dichalcogenide, with gap E_g driven with circularly polarized infrared light. The driving frequency Ω_F and the Fermi energy ε_F are chosen detuned, such that single photon absorption and particle-hole creation with energy transfer $\hbar\Omega_F$ is blocked by the Fermi sea. The driving leads to a change of the group velocity at the Fermi surface (red). b) This change results in a shift of the plasmon dispersion $\omega_{\text{pl}}(q)$. c) Modulating the amplitude of the Floquet drive with a frequency $\omega_1 \ll \Omega_F$ will lead to an oscillating Fermi velocity. This oscillation induces a parametric resonance of the plasmon modes. The spectrum of the modulated signal consists of a strong central peak at Ω_F and two side-bands at $\Omega_F \pm 2\omega_1$ (red peaks). The parametric generation of plasmons at half the difference frequency (blue peak) corresponds to frequency mixing.

Interesting effects on plasmon propagation can also be achieved with pulsed signals. In analogy to recent experiments with surface waves in classical liquids [20], we propose that pulses can be used to induce time reversal of propagating plasmon wave packets via a temporary change of the electrons' effective mass. A high frequency pulse will split a propagating plasmon wave packet into

two parts. While one part will continue to propagate in the initial direction, the other will evolve backwards in time and propagate towards the origin. We suggest that pulse induced time reversal is a promising way to control the propagation of THz plasmons with off-resonant, high frequency light, and discuss this functionality in more detail towards the end of this letter.

Modulated Floquet parametric driving: Floquet engineering of time varying materials. We now show, in more detail, how MFPD can be used to create a time varying plasmonic medium. Consider a gapped Dirac Hamiltonian which describes electrons near the Fermi level of a two dimensional material – e.g. a transition metal dichalcogenide or black phosphorus [67–69]:

$$H = \sum_{\mathbf{k}} \mathbf{c}_{\mathbf{k}}^\dagger [H_0(\mathbf{k}) + H_d(t)] \mathbf{c}_{\mathbf{k}} + \sum_{\mathbf{q}} V(\mathbf{q}) \rho_{\mathbf{q}} \rho_{-\mathbf{q}}. \quad (2)$$

We focus on a single valley and write $H_0 = \mathbf{d} \cdot \boldsymbol{\sigma}$ with $\mathbf{d} = [\lambda k_x, \lambda k_y, E_g/2]$, where, E_g is the energy gap between the two bands, $\boldsymbol{\sigma}$ is a Pauli vector describing pseudospin-orbit coupling, $\mathbf{c}_{\mathbf{k}}^\dagger, \mathbf{c}_{\mathbf{k}}$ are electron creation and annihilation operators, $\rho_{\mathbf{q}} = \sum_{\mathbf{k}} \mathbf{c}_{\mathbf{k}+\mathbf{q}}^\dagger \mathbf{c}_{\mathbf{k}}$ is the density operator and $V(\mathbf{q}) = 2\pi/q$ is the 2D Fourier transform of the Coulomb potential. The driving part of the Hamiltonian is derived from minimal coupling: $H_d(\mathbf{k}) = e\mathbf{A} \cdot \nabla_{\mathbf{k}} H_0$. We assume driving by circularly polarized light with an amplitude \mathcal{E} described by the vector potential $\mathbf{A} = (\mathcal{E}/\Omega_F) [-\sin \Omega_F t, \cos \Omega_F t, 0]$. Spin-valley degeneracy is included in the final results.

To avoid direct single photon absorptions, which are a dominant source of heating in Floquet engineered systems [36, 38, 70], we suggest to operate in an off-resonant regime, where the Fermi surface lies close to, but above the single photon resonance (see Fig.1). In this off-resonant regime, all states supporting excitations of a single electron by photons with an energy of $\hbar\Omega_F$ and near-zero momentum transfer are blocked. Processes involving the absorption of multiple photons are suppressed to second order in the small ratio of driving amplitude over driving frequency $e\mathcal{E}\lambda/\Omega_F^2 \hbar^2$ [38, 70]. Interaction and disorder assisted single photon absorption is possible, but can be shown to not cause an overheating of the system (see Supplement G).

Let us now carry out the MFPD program and subject the Floquet drive amplitude \mathcal{E} to a slow modulation. Expanding the dispersion relation around the Fermi momentum [71] we find $\varepsilon_k \approx \hbar v_F(\mathcal{E}, \Omega_F)(k - k_F) + \varepsilon_{k_F}(\mathcal{E}, \Omega_F)$ [72]. Here, the Fermi velocity $v_F(\mathcal{E}, \Omega_F)$ depends on the amplitude and frequency of the Floquet drive. A slow, adiabatic, time periodic modulation of \mathcal{E} according to $\mathcal{E}(t) = \bar{\mathcal{E}} + \delta\mathcal{E} \cos(2\omega_1 t)$, where $\omega_1 \ll \Omega_F$, will result in an oscillating Fermi velocity. For our purposes, it will be convenient to parametrize this time dependence as an oscillation of the effective mass $m^* = \hbar k_F / v_F(\mathcal{E}, \Omega_F)$:

$$m^*(t) = \bar{m}^* (1 + h \cos(2\omega_1 t)). \quad (3)$$

Here, h is a small dimensionless number quantifying the amplitude of the oscillatory component of the effective mass. Below, we estimate that for reasonable driving strengths h is of the order of 10^{-2} . Explicit formulas for $\varepsilon_k(\mathcal{E}, \Omega_F)$, $v_F(\mathcal{E}, \Omega_F)$ and $\bar{m}^*(\mathcal{E}, \Omega_F)$ are given in Supplement A.

Momentum-gapped states. We now investigate the influence of the oscillating effective mass of Eq. (3) on the dispersion relation of plasmons in a Coulomb interacting 2D electron gas. The plasmon dynamics can be inferred from charge and momentum conservation [73–76]. An inhomogeneous charge distribution $\rho(\mathbf{x}, t)$ will induce an electrostatic potential $\phi(\mathbf{x}, t)$ in the system, which will accelerate the electrons according to Newton's law: $\partial_t \mathbf{p}(\mathbf{x}, t) = -e\rho(\mathbf{x}, t) \nabla \phi(\mathbf{x}, t)$. Here, \mathbf{p} is the momentum density of the electrons. Combining the continuity equation $\partial_t \rho(\mathbf{x}, t) = -\nabla \cdot \mathbf{j}(\mathbf{x}, t)$ and the relationship between momentum and current densities $e\mathbf{p}(\mathbf{x}, t) = m^*(t)\mathbf{j}(\mathbf{x}, t)$ (see Supplement B) with Newton's law, we find

$$\partial_t m^*(t) \partial_t \rho(\mathbf{x}, t) = \frac{e}{4\pi\varepsilon} \nabla \cdot \rho(\mathbf{x}, t) \nabla \int d^2x' \frac{\rho(\mathbf{x}', t)}{|\mathbf{x} - \mathbf{x}'|}, \quad (4)$$

where the integral extends over the sample. We separate the oscillating part of ρ from the homogeneous background $\bar{\rho}$ and write $\rho = \bar{\rho} + \delta\rho$. Linearizing Eq. (4) in $\delta\rho$, and assuming plane-wave solutions $\delta\rho(\mathbf{x}) = \delta\rho_{\mathbf{q}} \exp(i\mathbf{q} \cdot \mathbf{x})$, we obtain Eq. (1).

The plasmon dispersion $\omega_{\text{pl}}(q)$ is given by

$$\omega_{\text{pl}}(q) = \sqrt{\frac{e\bar{\rho}}{4\pi\bar{m}^*\varepsilon} q^2 V(q)}. \quad (5)$$

$V(q)$ is the Fourier transform of the Coulomb potential.

Consider a quasi one-dimensional, waveguide-like setup of infinite length and width l , oriented parallel to the x -axis. For this strip geometry we find

$$V(q) \approx \int_0^l dy \int_{-\infty}^{\infty} dx \frac{e^{i\mathbf{q} \cdot \mathbf{x}}}{|\mathbf{x}|} \approx 2l \left| \ln \frac{|q|l}{4} \right| \quad (6)$$

for $q \ll 1/l$, where $\mathbf{q} = q\hat{\mathbf{e}}_x$. The precise geometry of the device is not very important for the physics presented here. The calculations would be very similar for an infinite 2D sample with $V(q) = 2\pi/q$, but we would need to keep track of the vector nature of \mathbf{q} .

Let us study the behavior of $\delta\rho_q$ in the vicinity of the parametric resonance, where $|\omega_{\text{pl}}(q) - \omega_1| \approx h\omega_1$. Using the ansatz $\delta\rho_q = a_q(t) \cos(\omega_1 t) + b_q(t) \sin(\omega_1 t)$, where the slowly varying coefficients are given by $a_q(t) = \tilde{a}e^{st}$ and $b_q(t) = \tilde{b}e^{st}$, we find (see Supplement C)

$$s_{\pm}(q) = \pm \frac{\omega_1}{2} \sqrt{\frac{1}{4}h^2 - \left(\frac{\omega_{\text{pl}}^2(q) - \omega_1^2}{\omega_1^2} \right)^2}. \quad (7)$$

For $|\omega_{\text{pl}}^2(q) - \omega_1^2| > \omega_1^2 h/2$ the exponent is imaginary, corresponding to dispersive plane-wave solutions,

whereas for $|\omega_{\text{pl}}^2(q) - \omega_1^2| < \omega_1^2 h/2$, we find exponentially growing (or decaying) unstable non-dispersive solutions oscillating at the frequency ω_1 . This results in a momentum gapped dispersion, similar to the one appearing in so called photonic time crystals [1, 15]. The gap is centered at the wavevectors $\pm q^*$, where q^* is determined by the resonance condition $\omega_{\text{pl}}(q^*) = \omega_1$.

Notice that Eq. (1) is invariant with respect to time translations by $T = \pi/\omega_1$. This symmetry is broken by the system's response – a feature that is known from discrete time crystals [77–83] and generic to parametric resonances. The momentum gap and the dispersion in the vicinity of the gap are shown in Fig. 2.

So far we did not consider the finite lifetime of plasmons. For small q , the plasmon dispersion lies outside the particle-hole continuum and Landau damping can be neglected (see Supplement G). In clean materials the main source of damping is momentum relaxing phonon scattering [84]. To model this effect, we add momentum decay at a rate γ to Newton's law $(\partial_t + \gamma) \mathbf{p}(\mathbf{x}, t) = -\rho(\mathbf{x}, t) \nabla \phi(\mathbf{x}, t)$. To first order in γ , $s_{\pm}(q)$ in Eq. (7) obtains a negative real part of $-\gamma/2$ (see Supplement C). The instability condition $\text{Re}(s_{\pm}) > 0$ is realized in a narrow region around q^* for

$$h > 2\gamma/\omega_1. \quad (8)$$

Interestingly, even if $h < 2\gamma/\omega_1$ holds, the momentum-gap remains intact. The gap then hosts non-dispersive modes with decay rates $-\gamma/2 \pm \omega_1 h^2/4$ at $q = q^*$.

Eq. (7) suggests that the opening of the momentum gap is associated with the joining of two branches of the plasmon dispersion described by the plus and minus signs. To interpret the two branches, it is useful to write the solution of Eq. (7) in the form known from Floquet's theorem [85]:

$$\delta\rho_q = e^{-i\varepsilon_{\text{pl}}(q)t} u_{\varepsilon_{\text{pl}}}(t), \quad (9)$$

where $\varepsilon_{\text{pl}}(q)$ is the plasmon quasi-dispersion that determines wave propagation once the periodic modulation is switched on [86], and $u_{\varepsilon_{\text{pl}}}(t) = e^{-i\varepsilon_{\text{pl}}t} [a(e^{2i(\varepsilon_{\text{pl},\pm} + is_{\pm})t} + 1) \pm ib(e^{2i(\varepsilon_{\text{pl},\pm} + is_{\pm})t} - 1)]/2$, where the plus is chosen for $\varepsilon_{\text{pl}} < 0$ and vice versa. It is easy to verify that $u_{\varepsilon_{\text{pl}}}(t + \pi/\omega_1) = u_{\varepsilon_{\text{pl}}}(t)$, in accordance with Floquet's theorem. The quasi-dispersion $\varepsilon_{\text{pl}}(q)$ can be confined to a Brillouin zone of width $2\omega_1$. We choose $\pm\omega_1$ as the boundaries of the Brillouin zone. Away from the gap, for small q , the dispersion is given by $\varepsilon_{\text{pl}}(q) \approx \pm i\omega_{\text{pl}}(q)/\sqrt{1 + h^2/4}$, showing that the impact of the drive is small. The plasmonic band structure in terms of ε_{pl} is shown in Fig. 2.

Production of entangled plasmon pairs. Since the momentum supplied by the optical drive is negligible, plasmons can only be produced in pairs with opposite momenta $\pm\hbar q$. This results in generation of entangled plasmon pairs. To see this, we find the Hamiltonian leading to Eq. (1) and then apply a second quantization proce-

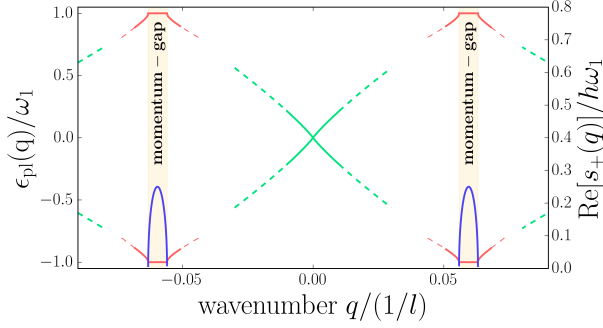


Figure 2. Dispersion of the plasmonic time varying medium. The modulated Floquet drive couples to plasmon modes and induces gaps (yellow segments) near the resonance $\omega_{\text{pl}}(q) = \pm\omega_1$. In the vicinity of the gaps, the modes are given by Eq. (7) (red curves). Away from the gap, the drive-induced changes to the dispersion are small (green curves) and Eqs. (5) and (6) are approximately valid. The growth rate of the unstable modes $\text{Re}[s_+(q)]$ is shown in blue.

ture following Refs. [13, 14]. Details are given in Supplement D. For the driven, resonant plasmon modes we find the Hamiltonian in the interaction representation

$$H_{\text{pl,int}} \approx \frac{\hbar}{4} \hbar\omega_1 \left(a_{q^*}^\dagger a_{-q^*}^\dagger + a_{-q^*} a_{q^*} \right), \quad (10)$$

where $a_{q^*}^\dagger$ and a_{q^*} are plasmon creation and annihilation operators for the resonant wavenumber q^* .

Applied to the vacuum, the time evolution operator $U_{\text{pl,int}}(t, 0) = \exp(-tH_{\text{pl,int}}/\hbar)$ generates a non-factorizable two mode squeezed state $|\psi_{\text{pl}}(t)\rangle = U_{\text{pl,int}}(t, 0)|0, 0\rangle$ in the basis $|n_q, n_{-q}\rangle$ [87], where n_q gives the number of plasmons in the state q . The generation of entangled plasmon pairs has been discussed previously in Ref. [88]. The authors suggested to excite the longitudinal plasmon modes of a graphene ribbon via their coupling to a resonantly pumped transverse mode and discussed modes of detection.

Pulse induced time reversal So far we have considered the action of a periodic oscillation of the effective mass $m^*(t)$ resulting from an amplitude modulated high frequency Floquet driving. We now discuss how a pulse induced, abrupt change of $m^*(t)$ can time reverse a propagating plasmon wave packet. The effect is shown in Fig.3. We consider a pulse with peak amplitude \mathcal{E}_0 , center frequency Ω_F and duration Δt . As shown in Supplement E, the effect of such a pulse at time $t = t_0$ on the effective mass can be described by the formula $m^*(t) = \bar{m}^* (1 + \bar{h}\delta(t - t_0))$, where \bar{h} is an amplitude characterizing the impact of the pulse. This assumes, that the pulse is very short compared to a plasmon oscillation cycle. For an incident wave packet $\delta\rho_i(\mathbf{x}, t)$, the time reversed part, which appears after the pulse, is given by (Supplement E)

$$\delta\rho_{\text{rev}}(\mathbf{x}, t) \approx A(q_0) \delta\rho_i(\mathbf{x}, -t). \quad (11)$$

Here, $A(q_0) = \frac{1}{2}\omega_{\text{pl}}(q_0)\bar{h}e^{-i2\omega_{\text{pl}}(q_0)t_0}$ is a complex amplitude and q_0 is the central wavenumber of the packet.

The assumption of a delta-function like, abrupt change of m^* , while convenient for analytic calculations (Supplement E), is only valid if the pulse duration is much shorter than the time scale of the plasmon oscillations. To achieve a strong reshaping of the electron dispersion, typically pulses with field strengths of $10^7 - 10^8$ V/m and durations of around 100 fs are employed [27, 30]. Being interested in the pulse induced time reversal of plasmons with frequencies of a few THz, we address the question of whether pulses with durations of up to half the plasmon oscillation cycle T_{pl} can be used. Using the Dedalus library [89], we carry out simulations (Supplementary E) for pulse durations of $\Delta t = 0.1T_{\text{pl}}$ (see Fig. 3), $\Delta t = 0.22T_{\text{pl}}$, and $\Delta t = 0.5T_{\text{pl}}$. We find that pulse induced time reversal is observable for all three values.

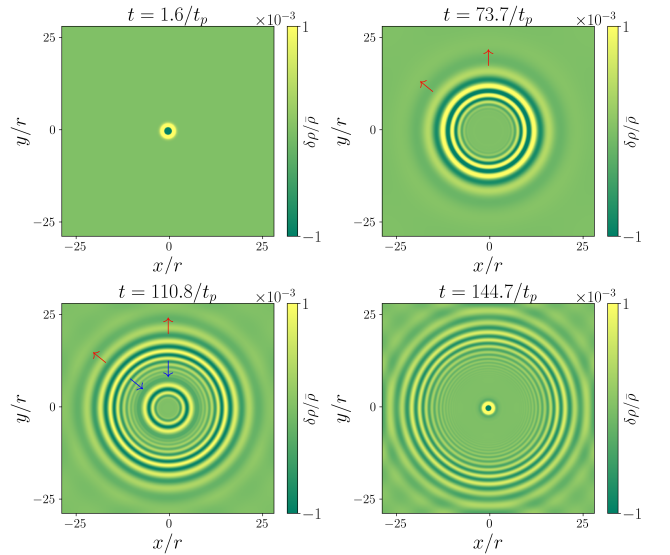


Figure 3. Numerical simulation of pulse induced time reversal of a propagating cylindrical plasmon wave packet. The plasmon is triggered by an electromagnetic pulse with duration t_p localized in a region with radius r around the origin. A high frequency gaussian pulse, resulting in a change of the electron's Fermi velocity and effective mass, is applied at time $t_0 = 75t_p$. The wavefront is splitted into parts, with the time-reversed part propagating back towards the origin (blue arrows). At $2t_0$, the time reversed front is focused back at the origin. For this simulation, Eq. (4) was solved using the Dedalus package [89].

Discussion. The reshaping of bandstructure by light in the off-resonant regime considered here has recently been demonstrated in doped black phosphorus [30], showing that the regime of operation for MFPD controlled plasmonic time varying materials is within experimental reach. In Supplement F, we estimate the critical driving strength to be $\bar{\mathcal{E}} \approx 4 \cdot 10^5$ V/m using Eq. (8) and the parameters $\bar{\rho} = 1.18 \cdot 10^{11}/\text{cm}^{-2}$, $E_g = 0.3$ eV, $\hbar\Omega_F = 0.35$ eV, $\lambda = 15$ eV \AA , $\epsilon = 6\epsilon_0$. The corresponding laser intensity is orders of magnitude smaller than in cur-

| sample | frequency | wavelength | field strength |
|-------------------------------|-----------|-------------------|----------------------|
| 2D | 1 THz | 8.2 μm | $2.3 \cdot 10^5$ V/m |
| 2D | 5 THz | 0.3 μm | $2.3 \cdot 10^5$ V/m |
| strip, $l = 0.2 \mu\text{m}$ | 1 THz | 1.7 μm | $1.6 \cdot 10^5$ V/m |
| strip, $l = 0.05 \mu\text{m}$ | 3 THz | 0.2 μm | $2.8 \cdot 10^5$ V/m |

Table I. Plasmon frequencies, wavelengths and field strengths of MFPD driven plasmons for a two dimensional and strip-like samples.

rent solid state Floquet experiments [27–30]. The choice of material parameters was inspired by black phosphorus, and can be adjusted for other materials. The estimate assumes a plasmon quality factor of $Q = \omega_1/\gamma \approx 10^2$, reachable in clean materials [24, 28, 84]. In theory, Q -factors of $10^3 - 10^4$ are believed to be achievable [84, 90], which would further reduce the necessary driving power. Moreover we demonstrate in Supplement G that the heating caused by photon absorption from MFPD can be compensated for by the cooling power of the lattice. We stress that the realization of plasmonic time reversal requires only pulsed signals and could be demonstrated with set-ups similar to the ones used in most Floquet experiments [27–30]. Near-field optical microscopy can be used for detection.

To estimate the experimental parameters, we consider plasmons with frequencies of 1 – 5 THz, and use the above values for material and driving parameters. Table I shows our estimates for plasmon wavelengths and field strengths. The momentum gap has typically a width of 1 – 2% of q^* , e.g. $0.05/\mu\text{m}$ for the strip and 1 THz. To estimate the field strengths, we draw on Ref. [52], which predicts that, due to nonlinear effects, the exponential plasmon growth saturates at amplitudes of $\sim \sqrt{8\hbar_c \bar{\rho}} \epsilon^{1/4}$, where ϵ is the relative distance of the drive from the critical driving strength. We assume a driving that is 10% above threshold, giving $\epsilon = 0.1$.

Summing up, we proposed a method to induce low frequency plasmons by amplitude modulated high frequency signals, and to create time varying materials for plasmons with effects such as parametric amplification, the opening of momentum gaps, time reversal mirroring, and creation of entangled plasmon pairs. The proposed effects can be measured with near field microscopy [58, 65, 66] and used in device applications, e.g. as plasmon sources or to control the propagation of plasmons.

ACKNOWLEDGMENTS

We acknowledge useful conversations with D. Basov and M. Rudner. E.K. thanks the Helen Diller quantum center for financial support.

SUPPLEMENTARY MATERIAL

A. Floquet engineering of the effective mass

The term Floquet engineering describes the willful tuning of the electron dispersion by a coherent, oscillating electromagnetic field. For the massive Dirac Hamiltonian of Eq. (2) considered in the letter, we find that the dispersion in the presence of an oscillating field with frequency Ω_F and amplitude \mathcal{E} , is given by

$$\varepsilon_k \approx \sqrt{\left(|\mathbf{d}| - \hbar \frac{\Omega_F}{2}\right)^2 + \frac{e^2 \mathcal{E}^2 \lambda^2}{4\Omega_F^2 \hbar^2} \left(2 - \frac{E_g}{|\mathbf{d}|}\right)}. \quad (\text{S1})$$

Here $|\mathbf{d}| = \sqrt{\lambda^2 k^2 + E_g^2/4}$. We assumed circularly polarized light described by the vector potential $\mathbf{A} = (\mathcal{E}/\Omega_F) [-\sin \Omega_F t, \cos \Omega_F t, 0]$. To derive Eq. (S1) we changed to the rotating frame by applying the unitary transformation $U = e^{i\hat{\mathbf{d}} \cdot \boldsymbol{\sigma} \Omega_F t}$ to Eq. (2) [26, 91] and used the rotating wave approximation, ignoring all terms oscillating at higher frequencies in the rotating frame [26, 91].

To find the effective mass, we first consider the Fermi velocity, which is given by

$$\begin{aligned} v_F(\mathcal{E}) &= \left. \frac{\partial \varepsilon_k}{\partial k} \right|_{k=k_F} \\ &= \frac{1}{\varepsilon_k} \left[\left(|\mathbf{d}| - \hbar \frac{\Omega_F}{2} \right) + \frac{e^2 \mathcal{E}^2 \lambda^2}{8\Omega_F^2 \hbar^2} \frac{E_g}{|\mathbf{d}|^2} \right] \left. \frac{\partial |\mathbf{d}|}{\partial k} \right|_{k=k_F} \\ &= \frac{1}{\varepsilon_{k_F}} \left[\left(|\mathbf{d}(k_F)| - \hbar \frac{\Omega_F}{2} \right) + \frac{e^2 \mathcal{E}^2 \lambda^2}{8\Omega_F^2 \hbar^2} \frac{E_g}{|\mathbf{d}(k_F)|^2} \right] \frac{\lambda^2 k_F}{|\mathbf{d}(k_F)|}. \end{aligned}$$

For the effective mass, we find

$$m^*(\mathcal{E}) = \frac{\hbar k_F}{v_F} = \frac{\hbar k_F}{\frac{1}{\varepsilon_{k_F}} \left[\left(|\mathbf{d}(k_F)| - \hbar \frac{\Omega_F}{2} \right) + \frac{e^2 \mathcal{E}^2 \lambda^2}{8\Omega_F^2 \hbar^2} \frac{E_g}{|\mathbf{d}(k_F)|^2} \right] \frac{\lambda^2 k_F}{|\mathbf{d}(k_F)|}}.$$

For an amplitude modulated driving of the form $\mathcal{E}(t) = \bar{\mathcal{E}} + \delta\mathcal{E} \cos(2\omega_1 t)$, the parameter h can be estimated as

$$h = \frac{1}{m^*(\bar{\mathcal{E}})} \frac{\partial m^*(\bar{\mathcal{E}})}{\partial \bar{\mathcal{E}}} \delta\mathcal{E}. \quad (\text{S2})$$

The behavior of the effective mass on the driving field strength \mathcal{E} is thus a complicated function of the material and driving parameters. In particular, it is non-analytic in $\mathcal{E} = 0$ for $|\mathbf{d}(k_F)| = \hbar \frac{\Omega_F}{2}$, where the electron quasi-dispersion exhibits a van-Hove singularity. As a rule of thumb, we find from Eq. (S2) that away from this singular point, the impact of the driving field on the effective mass, and consequently, the effect of the modulation of \mathcal{E} as parametrized by h , increases with a larger group velocity $v_g = \lambda/\hbar$, a small gap size E_g , and a smaller driving frequency Ω_F .

B. Momentum current relationship in a Dirac system

The relationship between current and momentum for a gapped Dirac Hamiltonian can be established using the Boltzmann transport theory for Fermi liquids. The Boltzmann equation for electrons reads [72]

$$\partial_t f_{\mathbf{k},\lambda} + v_{\mathbf{k},\lambda} \cdot \nabla f_{\mathbf{k},\lambda} = \mathcal{C}_{\text{coll}}[f]_{\mathbf{k},\lambda}, \quad (\text{S3})$$

with

$$f_{\mathbf{k},\lambda} = \frac{1}{1 + e^{\beta(\varepsilon_{\mathbf{k},\lambda} - \varepsilon_F - \hbar \mathbf{u} \cdot \mathbf{k})}}, \quad (\text{S4})$$

where $\varepsilon_{\mathbf{k},\lambda}$ and $v_{\mathbf{k},\lambda}$ are the electron dispersion and group velocity, respectively, λ is the band index, $\mathcal{C}_{\text{coll}}$ is the collision integral, and \mathbf{u} is the flow velocity of the electrons. In a metallic system as considered here, we can expand the dispersion relation around the Fermi energy ε_F , which lies in the upper band ($\lambda = +$):

$$\varepsilon_{\mathbf{k},\lambda} \approx \varepsilon_F + \hbar v_F (k - k_F). \quad (\text{S5})$$

To simplify the calculations, it is convenient to further approximate Eq. (S5) by a parabola, and write $\varepsilon_{\mathbf{k},\lambda} \approx \frac{\hbar^2 k^2}{2m^*} \approx \varepsilon_F + \frac{\hbar^2 k_F}{m^*} (k - k_F)$, where

$$m^* = \frac{\hbar k_F}{v_F}.$$

We can now calculate the momentum density of the system

$$\mathbf{p}(\mathbf{x}, t) = \sum_{\lambda} \int \frac{d^2 k}{(2\pi)^2} \hbar \mathbf{k} f_{\mathbf{k},\lambda} \quad (\text{S6})$$

$$= \int \frac{d^2 k}{(2\pi)^2} \hbar \mathbf{k} \frac{1}{1 + e^{\beta(\varepsilon_{\mathbf{k},+} - \varepsilon_F - \hbar \mathbf{u}(\mathbf{x}, t) \cdot \mathbf{k})}} \quad (\text{S7})$$

$$\approx \int \frac{d^2 k}{(2\pi)^2} \hbar \mathbf{k} \frac{1}{1 + e^{\beta\left(\frac{(\hbar \mathbf{k} - m^* \mathbf{u}(\mathbf{x}, t))^2}{2m^*} - \varepsilon_F - \frac{1}{2} m^* u^2(\mathbf{x}, t)\right)}} \quad (\text{S8})$$

$$\approx \int \frac{d^2 k}{(2\pi)^2} (\hbar \mathbf{k} + m^* \mathbf{u}(\mathbf{x}, t)) \frac{1}{1 + e^{\beta(\varepsilon_{\mathbf{k},+} - \varepsilon_F - \frac{1}{2} m^* u^2(\mathbf{x}, t))}}. \quad (\text{S9})$$

Since the distribution function does not depend on the angle of \mathbf{k} , the first term of the integrand cancels out. This leaves us, to leading order in the small u/v_F , with

$$\mathbf{p}(\mathbf{x}, t) = \bar{\rho} m^* \mathbf{u}(\mathbf{x}, t), \quad (\text{S10})$$

where $\bar{\rho}$ is the total electron density

$$\bar{\rho} = \int \frac{d^2 k}{(2\pi)^2} \frac{1}{1 + e^{\beta(\varepsilon_{\mathbf{k},+} - \varepsilon_F)}}. \quad (\text{S11})$$

A similar calculation can be carried out to find the current density. To first order in \mathbf{u} , we find

$$\begin{aligned} \mathbf{j}(\mathbf{x}, t) &= e \int \frac{d^2 k}{(2\pi)^2} \frac{1}{\hbar} \frac{\partial \varepsilon_{\mathbf{k},+}}{\partial \mathbf{k}} f_{\mathbf{k},\lambda} \\ &\approx e \int \frac{d^2 k}{(2\pi)^2} \frac{\hbar \mathbf{k}}{m^*} f_{\mathbf{k},\lambda} \\ &\approx e \bar{\rho} \mathbf{u}(\mathbf{x}, t). \end{aligned} \quad (\text{S12})$$

From Eqs. (S10) and (S12), we find

$$\mathbf{j}(\mathbf{x}, t) = \frac{e}{m^*} \mathbf{p}(\mathbf{x}, t),$$

which is the expression used to derive Eq. (4) of the main text.

C. Solving the time varying plasmon equation

Here we show details of our solution to Eq. (1) of the main text using the ansatz

$$\delta \rho = a(t) \cos(\omega_1 t) + b(t) \sin(\omega_1 t). \quad (\text{S13})$$

Inserting Eq. (S13) into Eq. (1) results in

$$\begin{aligned} \partial_t \left(1 + \frac{\delta m^*(t)}{m^*} \right) \partial_t \delta \rho &= -2\omega_1 h \sin(2\omega_1 t) \delta \dot{\rho} + (1 - h \cos(2\omega_1 t)) \delta \ddot{\rho} \\ &= -2\omega_1 h \sin(\omega_1 t) \left[\dot{a} \cos(\omega_1 t) + \dot{b} \sin(\omega_1 t) \right. \\ &\quad \left. - a\omega_1 \sin(\omega_1 t) + b\omega_1 \cos(\omega_1 t) \right] \\ &\quad + (1 - h \cos(2\omega_1 t)) \left[\ddot{a} \cos(\omega_1 t) + \ddot{b} \sin(\omega_1 t) \right. \\ &\quad \left. - 2\dot{a}\omega_1 \sin(\omega_1 t) + 2\dot{b}\omega_1 \cos(\omega_1 t) \right. \\ &\quad \left. - a\omega_1^2 \cos(\omega_1 t) - b\omega_1^2 \sin(\omega_1 t) \right] \end{aligned}$$

$$\begin{aligned}
\partial_t \left(1 + \frac{\delta m^*(t)}{m^*} \right) \partial_t \delta \rho \approx & -\omega_1 h \left[\dot{a} \sin(\omega_1 t) + \dot{b} \cos(\omega_1 t) \right. \\
& - a \omega_1 \cos(\omega_1 t) + b \omega_1 \sin(\omega_1 t) \\
& + \left[\ddot{a} \cos(\omega_1 t) + \ddot{b} \sin(\omega_1 t) \right. \\
& - 2\dot{a} \omega_1 \sin(\omega_1 t) + 2\dot{b} \omega_1 \cos(\omega_1 t) \\
& \left. \left. - a \omega_1^2 \cos(\omega_1 t) - b \omega_1^2 \sin(\omega_1 t) \right] \right. \\
& + (h/2) \left[\ddot{a} \cos(\omega_1 t) - \ddot{b} \sin(\omega_1 t) \right. \\
& + 2\dot{a} \omega_1 \sin(\omega_1 t) + 2\dot{b} \omega_1 \cos(\omega_1 t) \\
& \left. \left. - a \omega_1^2 \cos(\omega_1 t) + b \omega_1^2 \sin(\omega_1 t) \right]
\end{aligned}$$

$$\begin{aligned}
\gamma \partial_t \delta \rho = \gamma \left[\dot{a} \cos(\omega_1 t) + \dot{b} \sin(\omega_1 t) \right. \\
\left. - a \omega_1 \sin(\omega_1 t) + b \omega_1 \cos(\omega_1 t) \right].
\end{aligned}$$

Comparing the coefficients in front of the sine and cosine functions we find the equations for the amplitudes $a(t)$ and $b(t)$:

$$\begin{aligned}
-\omega_1 h (\dot{a} + \omega_1 b) + \ddot{b} - 2\dot{a} \omega_1 - b \omega_1^2 + (h/2) (-\ddot{b} + 2\dot{a} \omega_1 + b \omega_1^2) + \gamma (\dot{b} - a \omega_1) + \omega_{\text{pl}}^2(q) b = 0 \\
-\omega_1 h (\dot{b} - \omega_1 a) + \ddot{a} + 2\dot{b} \omega_1 - a \omega_1^2 + (h/2) (\ddot{a} + 2\dot{b} \omega_1 - a \omega_1^2) + \gamma (\dot{a} + b \omega_1) + \omega_{\text{pl}}^2(q) a = 0
\end{aligned}$$

anticipating $a \sim b \sim e^{st}$, where $s \sim \omega_1 h$ and ignoring $\mathcal{O}(h^2)$ and higher, we find

$$\begin{aligned}
-\omega_1^2 h b / 2 - 2\dot{a} \omega_1 - \gamma a \omega_1 + (\omega_{\text{pl}}^2(q) - \omega_1^2) b = 0 \\
\omega_1^2 h a / 2 + 2\dot{b} \omega_1 + \gamma b \omega_1 + (\omega_{\text{pl}}^2(q) - \omega_1^2) a = 0.
\end{aligned} \tag{S 14}$$

Next we use the ansatz $a = \tilde{a} e^{st}$, $b = \tilde{b} e^{st}$:

$$\begin{bmatrix} -2s\omega_1 - \gamma\omega_1 & -\frac{1}{2}\omega_1^2 h + (\omega_{\text{pl}}^2 - \omega_1^2) \\ \frac{1}{2}\omega_1^2 h + (\omega_{\text{pl}}^2 - \omega_1^2) & 2s\omega_1 + \gamma\omega_1 \end{bmatrix} \begin{bmatrix} a \\ b \end{bmatrix} = 0.$$

The solvability condition

$$-(2s + \gamma)^2 - \frac{(\omega_{\text{pl}}^2 - \omega_1^2)^2}{\omega_1^2} + \left(\frac{1}{2} \omega_1 h \right)^2 = 0$$

gives

$$s = -\frac{\gamma}{2} \pm \frac{1}{2} \sqrt{\left(\frac{1}{2} \omega_1 h \right)^2 - \frac{(\omega_{\text{pl}}^2 - \omega_1^2)^2}{\omega_1^2}}.$$

This corresponds to Eq. (7) of the main text. The condition of instability is $s > 0$:

$$\gamma < \sqrt{\left(\frac{1}{2} \omega_1 h \right)^2 - \frac{\epsilon^4}{\omega_1^2}},$$

thus plasmons in the frequency region

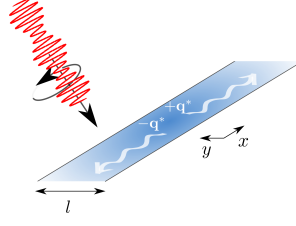
$$\epsilon^4 < \frac{1}{4} \omega_1^4 h^2 - \omega_1^2 \gamma^2$$

will become unstable if

$$h > \frac{2\gamma}{\omega_1}.$$

The instability grows according to

$$\delta \rho \sim e^{(h\omega_1/4 - \gamma/2)t}. \tag{S 15}$$



Supplementary Figure S 1. Quasi one-dimensional strip geometry considered in Eq. (6). Due to momentum conservation, plasmons created by MFPD come in entangled pairs with momenta $\pm q^*$.

D. Production of entangled plasmon pairs

Eq (1) of the main text – the equation of motion for the charge density – can be derived from the Hamiltonian

$$H_{\text{pl}} = \sum_{\mathbf{q}} \frac{1}{2} (1 + h \cos(2\omega_1 t))^{-1} p_{\mathbf{q}} p_{-\mathbf{q}} + \frac{1}{2} \omega_{\text{pl}}^2(\mathbf{q}) \delta\rho_{\mathbf{q}} \delta\rho_{-\mathbf{q}} \quad (\text{S 16})$$

using Hamilton's equations:

$$\begin{aligned} \partial_t \delta\rho_{\mathbf{q}} &= \frac{\partial H}{\partial p_{\mathbf{q}}} = \frac{p_{-\mathbf{q}}}{1 + h \cos(2\omega_1 t)} \\ \partial_t p_{\mathbf{q}} &= -\frac{\partial H}{\partial \delta\rho_{\mathbf{q}}} = -\omega_{\text{pl}}^2(\mathbf{q}) \delta\rho_{-\mathbf{q}}. \end{aligned} \quad (\text{S 17})$$

In the following, we focus on the quasi-1D geometry of Fig.S 1 where the wavevectors \mathbf{q} are replaced by the wavenumbers $\pm q$. We subject the Hamiltonian (S 16) to canonical quantization. Creation and annihilation operators are defined as

$$\begin{aligned} a_q &= \sqrt{\frac{\omega_{\text{pl}}(q)}{2\hbar}} \left(\delta\rho_q - \frac{p_{-q}}{i\omega_{\text{pl}}(q)} \right) \\ a_q^\dagger &= \sqrt{\frac{\omega_{\text{pl}}(q)}{2\hbar}} \left(\delta\rho_{-q} + \frac{p_q}{i\omega_{\text{pl}}(q)} \right), \end{aligned} \quad (\text{S 18})$$

and canonical quantization is implemented by demanding

$$[a_q, a_{q'}^\dagger] = \delta_{q, q'}. \quad (\text{S 19})$$

Written in terms of creation and annihilation operators, the Hamiltonian of Eq. (S 16) reads

$$\begin{aligned} H &= \sum_q \frac{\hbar\omega_{\text{pl}}(q)}{4} \left(1 + \frac{1}{1 + h \cos(2\omega_1 t)} \right) \left(a_q^\dagger a_q + a_{-q}^\dagger a_{-q} \right) \\ &+ \frac{\hbar\omega_{\text{pl}}(q)}{4} \left(\frac{h \cos(2\omega_1 t)}{1 + h \cos(2\omega_1 t)} \right) \left(a_q^\dagger a_{-q}^\dagger + a_{-q} a_q \right). \end{aligned} \quad (\text{S 20})$$

Focusing on the resonant mode with $q = q^*$, for a small modulation strength $h \ll 1$, we find

$$H_{\text{pl, int}} \approx \frac{\hbar}{4} \hbar\omega_1 \left(a_{q^*}^\dagger a_{-q^*}^\dagger + a_{-q^*} a_{q^*} \right) \quad (\text{S 21})$$

for the Hamiltonian in the interaction representation.

Applying the time evolution operator $U_{\text{pl, int}}(t, 0) = \exp(-tH_{\text{pl, int}}/\hbar)$ to the vacuum generates a non-factorizable two mode squeezed state $|\psi_{\text{pl}}(t)\rangle = U_{\text{pl, int}}(t, 0)|0, 0\rangle$ in the basis $|n_q, n_{-q}\rangle$ [87]. Here, n_q is the number of plasmons in the state q :

$$|\psi_{\text{pl}}(t)\rangle = \frac{1}{\cosh\left(\frac{\hbar\omega_1 t}{4}\right)} \sum_{n=0}^{\infty} \tanh^n\left(\frac{\hbar\omega_1 t}{4}\right) |n_q, n_{-q}\rangle. \quad (\text{S 22})$$

The total number of plasmons is given by

$$\langle N_{\pm q} \rangle = \langle \psi_{\text{pl}}(t) | a_{\pm q}^\dagger a_{\pm q} | \psi_{\text{pl}}(t) \rangle. \quad (\text{S 23})$$

We find

$$\langle N_{\pm q} \rangle = \sinh^2 \left(\frac{\hbar\omega_1 t}{4} \right) \sim \exp \left(\frac{\hbar\omega_1 t}{2} \right), \quad (\text{S } 24)$$

which means that the intensity of the plasmon fields grows in accordance with the classical result of Eq. (7) of the main text.

E. Pulse induced time reversal

Let us consider an optical pulse with frequency Ω_F and envelope $\mathcal{E}(t) = \mathcal{E}_0 f(t - t_0)$, such that the maximum amplitude \mathcal{E}_0 is reached at t_0 . Let the pulse have a width Δt , which is chosen such that $2\pi/\Omega_F \ll \Delta t \ll 2\pi/\omega_{\text{pl}}(q_0)$, where $\omega_{\text{pl}}(q_0)$ is the central frequency of the plasmon wave packet. The dependence of the effective mass on \mathcal{E} is given by the formula

$$m^*(t) = \left. \frac{\varepsilon_k(\mathcal{E}(t), \Omega_F)}{\lambda k_F^2 \left(1 - \frac{\hbar\Omega_F}{2|\mathbf{d}|}\right)} \right|_{k=k_F}. \quad (\text{S } 25)$$

For simplicity, we can assume that

$$f(t) = \Theta(t - \Delta t/2) \Theta(t + \Delta t/2), \quad (\text{S } 26)$$

which translates to

$$m^*(t) = \bar{m}^* + f(t) \left. \frac{\varepsilon_k(\mathcal{E}_0, \Omega_F)}{\lambda k_F^2 \left(1 - \frac{\hbar\Omega_F}{2|\mathbf{d}|}\right)} \right|_{k=k_F}. \quad (\text{S } 27)$$

If the pulse is very short with $\Delta t \ll 2\pi/\omega_{\text{pl}}(q_0)$, we can further approximate it with a delta function: $f(t) \approx \Delta t \delta(t - t_0)$. This yields

$$m^*(t) = \bar{m}^* + \Delta t \delta(t - t_0) \left. \frac{\varepsilon_k(\mathcal{E}_0, \Omega_F)}{\lambda k_F^2 \left(1 - \frac{\hbar\Omega_F}{2|\mathbf{d}|}\right)} \right|_{k=k_F}. \quad (\text{S } 28)$$

Remembering that, although the pulse is short at the plasmon time-scale, it is actually long compared to $2\pi/\Omega_F$, we can write

$$m^*(t) = \bar{m}^* (1 + \bar{h} \delta(t - t_0)), \quad (\text{S } 29)$$

where

$$\bar{h} = \left. \frac{\Delta t \varepsilon_k(\mathcal{E}_0, \Omega_F)}{\lambda \bar{m}^* k_F^2 \left(1 - \frac{\hbar\Omega_F}{2|\mathbf{d}|}\right)} \right|_{k=k_F} \quad (\text{S } 30)$$

is an amplitude characterizing the pulse. Thus, for a single driving pulse, Eq. (1) becomes

$$\partial_t^2 \delta \rho_{\mathbf{q}} + \omega_{\text{pl}}^2(q) \delta \rho_{\mathbf{q}} = -\bar{h} \partial_t \delta(t - t_0) \partial_t \delta \rho_{\mathbf{q}}. \quad (\text{S } 31)$$

For $t < t_0$, we consider a propagating wave-packet of the form

$$\delta \rho_i(\mathbf{x}, t) = \int \frac{d^2 q}{2\pi} \phi_i(\mathbf{q}) e^{i\mathbf{q} \cdot \mathbf{x} - i\omega_{\text{pl}}(q)t}, \quad (\text{S } 32)$$

which is a linear superposition of solutions to the homogeneous part of Eq. (S 31). For $t \geq t_0$, we write

$$\delta \rho(\mathbf{x}, t) = \int \frac{d^2 q}{2\pi} \phi(\mathbf{q}) e^{i\mathbf{q} \cdot \mathbf{x} - i\omega_{\text{pl}}(q)t} \quad (\text{S } 33)$$

To find the solution for $t > t_0$, we use the retarded Green's function

$$G_R(t) = \Theta(t) \frac{\sin(\omega(q)t)}{\omega(q)}, \quad (\text{S } 34)$$

which fulfills

$$\partial_t^2 G_R(t) + \omega_{\text{pl}}^2(q) G_R(t) = \delta(t). \quad (\text{S } 35)$$

From this expression, it is evident that a solution to Eq. (S 31) is given by

$$-i \int \frac{d^2 q}{2\pi} \int_{-\infty}^{\infty} dt' [\partial_{t'} G_R(t-t')] \bar{h} \delta(t'-t_0) \phi(\mathbf{q}) \omega_{\text{pl}}(q) e^{i\mathbf{q}\cdot\mathbf{x} - i\omega_{\text{pl}}(q)t'} \quad (\text{S } 36)$$

where we used integration by parts. In the above equation, the term involving the derivative of the Heaviside function inside G_R vanishes, and we are left with

$$\begin{aligned} & i \int \frac{d^2 q}{2\pi} \Theta(t-t_0) \cos(\omega(q)(t-t_0)) \bar{h} \omega_{\text{pl}}(q) \phi(\mathbf{q}) e^{i\mathbf{q}\cdot\mathbf{x} - i\omega_{\text{pl}}(q)t_0} \\ & = \frac{i}{2} \bar{h} \Theta(t-t_0) \partial_t [\delta\rho(\mathbf{x}, 2t_0 - t) + \delta\rho(\mathbf{x}, t)] \end{aligned} \quad (\text{S } 37)$$

The full solution is the sum of the homogeneous and pulse induced parts:

$$\delta\rho(\mathbf{x}, t) = \delta\rho_i(\mathbf{x}, t) + \frac{i}{2} \bar{h} \Theta(t-t_0) \partial_t [\delta\rho(\mathbf{x}, 2t_0 - t) + \delta\rho(\mathbf{x}, t)]. \quad (\text{S } 38)$$

Eq. (S 38) is a self consistent equation and can be solved by iteration. To first order in \bar{h} , we find

$$\delta\rho(\mathbf{x}, t) \approx \delta\rho_i(\mathbf{x}, t) + \frac{i}{2} \bar{h} \Theta(t-t_0) \partial_t [\delta\rho_i(\mathbf{x}, 2t_0 - t) + \delta\rho_i(\mathbf{x}, t)] \quad (\text{S } 39)$$

The time inverted, backwards propagating wave is given by

$$\delta\rho_{\text{rev}}(\mathbf{x}, t) \approx \frac{i}{2} \bar{h} \Theta(t-t_0) \partial_t \delta\rho_i(\mathbf{x}, 2t_0 - t). \quad (\text{S } 40)$$

For a narrow packet, where $\phi(\mathbf{q})$ is centered around a wavenumber q_0 , and has a width Δq , expanding to leading order in $\Delta q/q_0$, we have

$$\delta\rho_{\text{rev}}(\mathbf{x}, t) \approx A(q_0) \delta\rho_i(\mathbf{x}, -t) \quad (\text{S } 41)$$

with a complex time-inversion amplitude

$$A(q_0) = \frac{1}{2} \omega_{\text{pl}}(q_0) \bar{h} e^{-i2\omega_{\text{pl}}(q_0)t_0}. \quad (\text{S } 42)$$

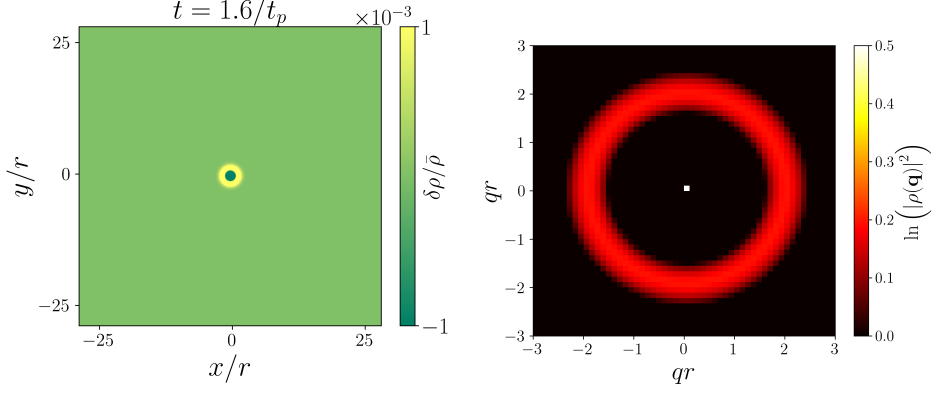
To explore the time-reversal effect in more detail and to consider pulse durations which are more realistic than the infinitely short pulse assumed above, we solve Eq. (4) numerically. To create a cylindrical we use a potential of the form

$$\phi(\mathbf{x}, t) = C e^{-\frac{x^2+y^2}{r^2}} t e^{-t/t_p}.$$

Here r can be thought of as the radius of a tip used to force the system and t_p measures the duration of the pulse. At time $t_0 = 75t_p$, we apply a strong sudden change of the effective mass:

$$m^*(t) = \bar{m}^* \left(1 + \bar{h} e^{-t^2/\Delta t^2} \right).$$

We explore the effect of different pulse durations Δt to the time-reversed signal. It is important to compare Δt to the characteristic frequency range of the plasmon signal to which pulse-induced time-reversal is applied. To this end, we perform a Fourier transform of the signal at $t = 3t_p$. The result is shown in Fig. S 2. The plasmon wavenumbers are roughly peaked around $qr = 1.9$. This means that the plasmon wavelength is roughly set by the diameter of the tip.



Supplementary Figure S 2. Plasmon wave at $t = 3t_p$ and its Fourier transform.

Using the dispersion relation of Eq. (5), we find that a wavenumber of $qr = 1.9$ corresponds to an oscillation cycle of $T_{\text{pl}}(q) = 2\pi/\omega_{\text{pl}}(q) \approx 10t_p$.

We run simulations with $\Delta t = 0.1T_{\text{pl}}$ and $\Delta t = 0.22T_{\text{pl}}$ with $\bar{h} = 1$ and $\Delta t = 0.5T_{\text{pl}}$ with $\bar{h} = 0.2$. Our main goal was to establish whether a pulse whose duration is not by orders of magnitude smaller than the oscillation period of the plasmon wave can induce time reversal. We find that for all pulse durations Δt , time reversal is clearly observable (see Fig. S 3), although the wavefront is distorted for $\Delta t = 0.5T_{\text{pl}}$. We conclude that pulse induced time reversal is quite robust to the duration of the pulse as compared to the duration of one oscillation cycle of the plasmon wave, and that time inversion is observable for a pulse which is half as long as the oscillation cycle. In fact, in recent experiments the time reversal of optical signals was measured for pulse durations comparable to the duration of one optical cycle.

F. Estimating the critical driving strength

We assume a gap size of $E_g = 0.3 \text{ eV}$, a Floquet driving frequency of $\hbar\Omega_F = 0.35 \text{ eV}$ and a pseudospin-orbit coupling of $\lambda = 15 \text{ eV}\text{\AA}$. An electron density of $\bar{\rho} = 1.18 \cdot 10^{11}/\text{cm}^{-2}$ guarantees that the Fermi energy is close to, but above the resonance. The plasmon quality factor Q sets a lower bound on the required driving and modulation strength. Assuming $Q = \omega_1/\gamma \approx 10^2$, the instability condition $\hbar > 2\gamma/\omega_1$ yields a critical driving strength of $\bar{\mathcal{E}} \approx 4 \cdot 10^5 \text{ V/m}$ with a modulation amplitude $\delta\bar{\mathcal{E}} = 0.5\bar{\mathcal{E}}$. Such field strengths can be reached with continuous wave lasers. The corresponding intensity is by a factor of 10^4 smaller than in current solid state Floquet engineering experiments [27–30].

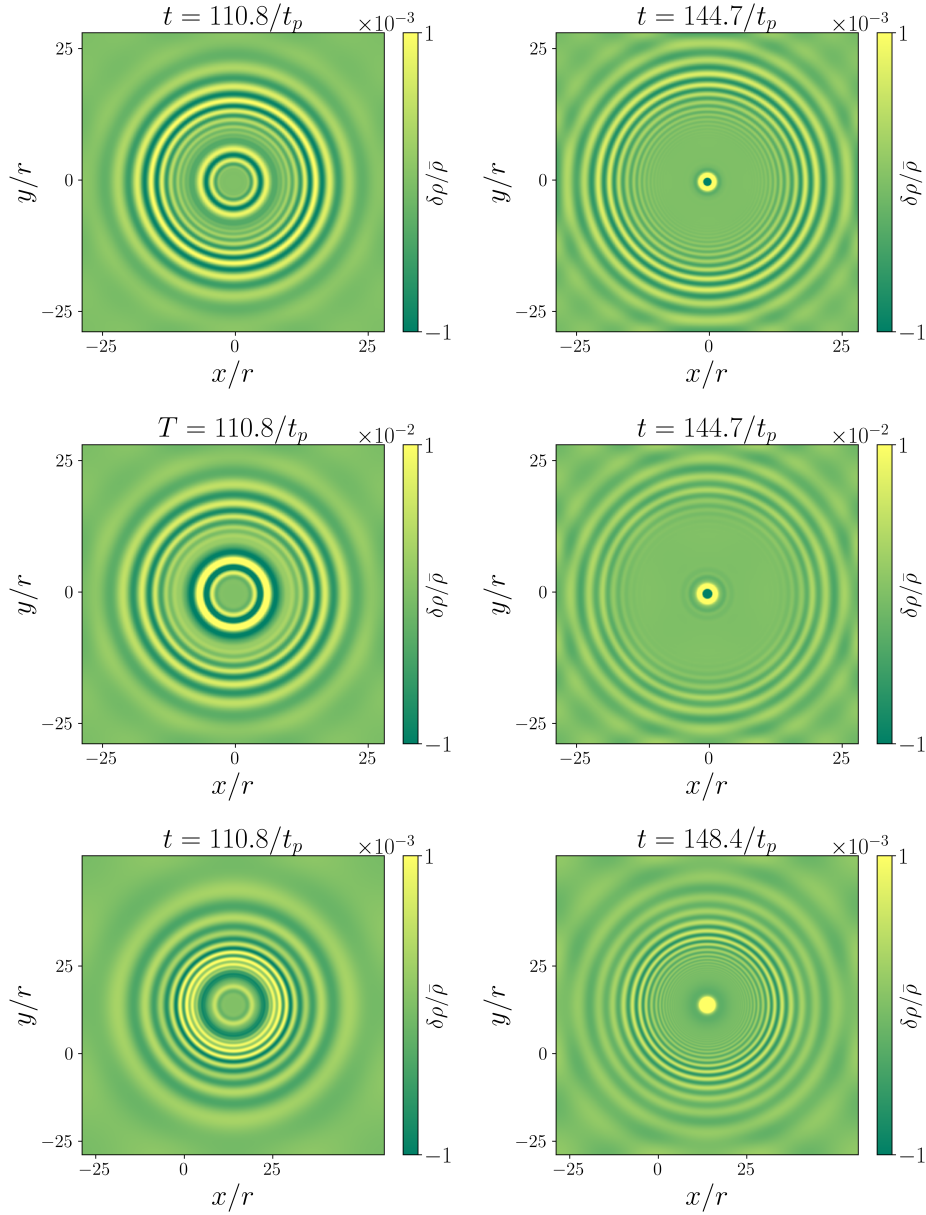
G. Heating and Landau damping

In undoped gapped systems, the main heating mechanisms are radiative recombination and momentum conserving single photon absorption [38, 70]. In the proposed set-up, these processes are suppressed by the exclusion principle. The most relevant allowed heating processes are phonon- or disorder-assisted, momentum non-conserving single-photon absorption and interaction-assisted single-photon absorption. Here we estimate the heating due to these processes and show that the Landau damping induced by this heating is very small.

In the following we calculate the number of electrons excited by momentum non-conserving single-photon absorptions per unit of time and area Γ_γ , and the corresponding number for interaction-aided single-photon absorptions Γ_{int} .

1. Estimation of Γ_γ

The matrix element for the absorption of n photons is proportional to $(e\mathcal{E}\lambda/\hbar\Omega_F^2)^n$ (see, e.g., [38]) and the rate of momentum non-conserving scattering is γ . Thus, according to Fermi's Golden rule, the scattering rate can be estimated as $\gamma(e\mathcal{E}\lambda/\hbar\Omega_F^2)^{2n}$. To find Γ_γ , we have to multiply by the density of electrons available for this kind of



Supplementary Figure S 3. Pulse induced time reversal with a pulse duration of $\Delta t = 0.1T_{p1}$ (first row), $\Delta t = 0.22T_{p1}$ (second row) and $\Delta t = 0.5T_{p1}$ (third row). The pulse was triggered at $t = 75t_p$. The inner concentric circles represent the time-reversed wave. For $\Delta t = 0.5T_{p1}$, we observe a strong interference of the forward and backward propagating waves, however, a time-reversed signal is clearly observable at $t \approx 150t_p$.

scattering. Slightly overestimating this density (and the heating due to this process), we approximate it by the total electron density of the upper band $\rho = \pi k_F^2 / (2\pi)^2$. We thus find

$$\Gamma_\gamma \approx \frac{\gamma \pi k_F^2}{(2\pi)^2} \left(\frac{e\mathcal{E}\lambda}{\hbar\Omega_F^2} \right)^2. \quad (\text{S } 43)$$

Using the estimates from the main text ($\hbar\Omega_F = 0.35 \text{ eV}$, $\lambda = 15 \text{ eV\AA}$, $\bar{\mathcal{E}} \approx 4 \cdot 10^5 \text{ V/m}$), the dimensionless amplitude of the electric field controlling the strength of the photon absorption is

$$\frac{e\mathcal{E}\lambda}{\hbar\Omega_F^2} \approx 5 \cdot 10^{-3}.$$

We find

$$\begin{aligned}\Gamma_\gamma &\approx 2.5 \cdot 10^{-5} \cdot \gamma \rho \\ &\approx 1.6 \cdot 10^6 \text{Hz} \cdot \rho.\end{aligned}$$

We assumed $\gamma \approx 6.28 \cdot 10^{10} \text{Hz}$ for a quality factor $Q = \omega/\gamma = 10^2$ and a plasmon frequency of $\omega/2\pi = 1 \text{THz}$.

2. Estimation of Γ_{int}

In this process, a single photon is absorbed and its energy is distributed between two electrons. The two electrons exchange a momentum \mathbf{q} through Coulomb interaction. Energy conservation yields

$$\varepsilon(\mathbf{k}_1 + \mathbf{q}) + \varepsilon(\mathbf{k}_2 - \mathbf{q}) - \varepsilon(\mathbf{k}_2) - \varepsilon(\mathbf{k}_1) - \hbar\Omega_F = 0.$$

Thus, the available phase space for this process is very limited. The Coulomb potential is given by

$$V(\mathbf{q}) = \frac{e^2}{\varepsilon} \frac{2\pi}{q + q_s},$$

where the screening length is $q_s \approx 4\alpha k_F$, with the fine structure constant $\alpha = e^2/\varepsilon\lambda$ [92]. This approximation is valid when the Fermi energy is far enough from the bottom of the band and the dispersion is nearly linear. For the estimate at hand, we approximate

$$\begin{aligned}V(0) &\approx \frac{e^2}{\varepsilon} \frac{2\pi}{q_s} \\ \varepsilon(\mathbf{k}) &\approx \lambda k\end{aligned}$$

The number of absorbed photons per unit of time can then be estimated using Fermi's Golden rule as

$$\Gamma_{\text{int}} \approx \frac{1}{\hbar} \int \frac{d^2 k_1}{(2\pi)^2} \int \frac{d^2 k_2}{(2\pi)^2} \int \frac{d^2 q}{(2\pi)^2} \delta(\varepsilon(\mathbf{k}_1 + \mathbf{q}) + \varepsilon(\mathbf{k}_2 - \mathbf{q}) - \varepsilon(\mathbf{k}_2) - \varepsilon(\mathbf{k}_1) - \hbar\Omega_F) V^2(0) \left(\frac{e\mathcal{E}\lambda}{\hbar\Omega_F^2} \right)^2.$$

To take the integrals, it is useful to introduce dimensionless variables

$$\begin{aligned}\mathbf{K}_i &= \mathbf{k}_i/k_F \\ \mathbf{Q} &= \mathbf{q}/k_F \\ \bar{\Omega} &= \hbar\Omega_F/\lambda k_F\end{aligned}$$

The above integral can then be written as

$$\Gamma_{\text{int}} = \frac{V^2(0) k_F^6}{\lambda \hbar k_F} \left(\frac{e\mathcal{E}\lambda}{\hbar\Omega_F^2} \right)^2 \int \frac{d^2 K_1}{(2\pi)^2} \int \frac{d^2 K_2}{(2\pi)^2} \int \frac{d^2 Q}{(2\pi)^2} \delta(|\mathbf{K}_1 + \mathbf{Q}| + |\mathbf{K}_2 - \mathbf{Q}| - |\mathbf{K}_2| - |\mathbf{K}_1| - \bar{\Omega}).$$

The q integration can be performed by going to elliptical coordinates. This procedure (for details see e.g. [93]) yields

$$\Gamma_{\text{int}} = \frac{V^2(0) k_F^5}{\hbar\lambda} \left(\frac{e\mathcal{E}\lambda}{\hbar\Omega_F^2} \right)^2 \int \frac{d^2 K_1}{(2\pi)^2} \int \frac{d^2 K_2}{(2\pi)^2} \int \frac{d\vartheta}{(2\pi)^2} |\mathbf{K}_1 + \mathbf{K}_2| \frac{\left(\frac{K_1 + K_2 + \bar{\Omega}}{|\mathbf{K}_1 + \mathbf{K}_2|} \right)^2 - \cos^2 \vartheta}{4\sqrt{\left(\frac{K_1 + K_2 + \bar{\Omega}}{|\mathbf{K}_1 + \mathbf{K}_2|} \right)^2 - 1}}.$$

For the parameters of our estimate ($\hbar\Omega = 0.35 \text{eV}$, $\lambda = 15 \text{eV}\text{\AA}$, $\bar{\mathcal{E}} \approx 4 \cdot 10^5 \text{V/m}$, $k_F = 1.2 \cdot 10^8 \text{m}^{-1}$), we find

$$\bar{\Omega} = 1.9.$$

A numerical evaluation of the remaining integral gives

$$\begin{aligned}\Gamma_{\text{int}} &\approx 1.02 \cdot 10^{-3} \cdot \frac{V^2(0) k_F^5}{\hbar\lambda} \left(\frac{e\mathcal{E}\lambda}{\hbar\Omega_F^2} \right)^2 \\ &= 1.02 \cdot 10^{-3} \cdot \frac{V^2(0) k_F^5}{\hbar\lambda} \left(\frac{e\mathcal{E}\lambda}{\hbar\Omega_F^2} \right)^2\end{aligned}$$

On the other hand

$$V(0) \approx \frac{e^2 \pi}{2 \varepsilon \alpha k_F}.$$

Collecting everything and assuming $\varepsilon = 6\varepsilon_0$, we find (SI Units)

$$\begin{aligned} \Gamma_{\text{int}} &\approx 1.02 \cdot 10^{-3} \cdot \frac{\pi e^4 k_F^3}{16 \hbar \varepsilon^2 \alpha^2 \lambda} \left(\frac{e \mathcal{E} \lambda}{\hbar \Omega_F^2} \right)^2 \\ &\approx 6.1 \cdot 10^6 \text{ Hz} \cdot \rho, \end{aligned}$$

where we used our estimate

$$\frac{e \mathcal{E} \lambda}{\hbar \Omega_F^2} \approx 5 \cdot 10^{-3}.$$

3. Landau damping

The Landau damping of plasmons is described by the imaginary part of the Lindhard function

$$\chi(\omega, \mathbf{q}) = \int \frac{d^2 k}{(2\pi)^2} \frac{f(\varepsilon_{\mathbf{k}-\mathbf{q}/2}) - f(\varepsilon_{\mathbf{k}+\mathbf{q}/2})}{\omega + i0^+ + \varepsilon_{\mathbf{k}-\mathbf{q}/2} - \varepsilon_{\mathbf{k}+\mathbf{q}/2}}.$$

The imaginary part is

$$\text{Im}[\chi(\omega, \mathbf{q})] = -\pi \int \frac{k dk}{(2\pi)^2} \int d\varphi [f(\varepsilon_{\mathbf{k}}) - f(\varepsilon_{\mathbf{k}+\mathbf{q}})] \delta(\omega + \varepsilon_{\mathbf{k}} - \varepsilon_{\mathbf{k}+\mathbf{q}}).$$

Let $\varepsilon_{\mathbf{k}} = k^2/2m^*$. This assumption simplifies the calculations but can be made without loss of generality, because in the end we only need to consider the linearized dispersion in the vicinity of the Fermi surface. Defining the quantities $\mathbf{K} = \mathbf{k}/\sqrt{2m^*}$, $\mathbf{Q}' = \mathbf{q}/\sqrt{2m^*}$, we have

$$\begin{aligned} \text{Im}[\chi(\omega, \mathbf{q})] &= -\pi \int \frac{k dk}{(2\pi)^2} \int d\varphi [f(K^2) - f(K^2 + Q'^2 + 2KQ' \cos \varphi)] \delta(Q'^2 + 2KQ' \cos \varphi - \omega) \\ &\quad - 2m^* \pi \int \frac{K dK}{(2\pi)^2} \int d\varphi [f(K^2) - f(K^2 + Q'^2 + 2KQ' \cos \varphi)] \delta\left(\frac{Q'^2 - \omega}{2KQ'} + \cos \varphi\right) \end{aligned}$$

We are interested in the case $\frac{Q'^2 - \omega}{2KQ'} < 0$, i.e. $-\pi/2 < \varphi < \pi/2$. We substitute

$$\begin{aligned} \mu &= \cos \varphi \\ d\varphi &= -\frac{d\mu}{\sin \varphi} = -\frac{d\mu}{\pm \sqrt{1 - \cos^2 \varphi}} \end{aligned}$$

where the plus-minus-sign indicates that we have to distinguish the cases $\varphi \lesseqgtr 0$. We find

$$\begin{aligned} \text{Im}[\chi(\omega, \mathbf{Q}')] &= -\frac{m^* \pi}{Q'} \int \frac{dK}{(2\pi)^2} \int_{-1}^1 \frac{d\mu}{\sqrt{1 - \mu^2}} [f(K^2) - f(K^2 + Q'^2 + 2KQ'\mu)] \delta\left(\frac{Q'^2 - \omega}{2KQ'} + \mu\right) \\ &= -\frac{m^* \pi}{Q'} \int_{\frac{\omega - Q'^2}{2Q'}}^{\infty} \frac{dK}{(2\pi)^2} \frac{1}{\sqrt{1 - \left(\frac{Q'^2 - \omega}{2KQ'}\right)^2}} [f(K^2) - f(K^2 + \omega)], \end{aligned} \quad (\text{S } 44)$$

where the last step follows from

$$-1 < \frac{Q'^2 - \omega}{2KQ'} < 0$$

For $T = 0$, approximating $f(K^2) - f(K^2 - \omega) \approx -\delta(K - K_F)\omega/K_F$, we find

$$\text{Im}[\chi(\omega, \mathbf{q})] = \frac{-m^*\omega}{4\pi Q K_F} \frac{\Theta\left(K_F - \frac{Q'^2 + \omega}{2Q}\right)}{\sqrt{1 - \frac{(Q'^2 - \omega)^2}{4K_F^2 Q'^2}}}$$

As the theta function indicates, plasmons are undamped for

$$\frac{qk_F}{m^*} < \omega - \frac{q^2}{2m}.$$

In our case $\omega \gg q^2/2m^*$ and the condition reduces to

$$\omega > v_F q.$$

At finite temperatures and with $\omega/Q' \gg Q'$, the integral in Eq. (S44) can be approximated as

$$\text{Im}[\chi(\omega, \mathbf{q})] \approx -\frac{m^*\pi}{Q'} \int_{\frac{\omega}{2Q'}}^{\infty} \frac{dK}{(2\pi)^2} \frac{K}{\sqrt{K^2 - \left(\frac{\omega}{2Q'}\right)^2}} [f(K^2) - f(K^2 + \omega)]$$

For $\omega \gg v_F q = K_F Q'/2$, we can approximate the Fermi-Dirac distributions as exponentials

$$\begin{aligned} \text{Im}[\chi(\omega, \mathbf{q})] &\approx -\frac{m^*\pi}{Q'} \int_{\frac{\omega}{2Q'}}^{\infty} \frac{dK}{(2\pi)^2} \frac{K}{\sqrt{K^2 - \left(\frac{\omega}{2Q'}\right)^2}} [e^{-\beta K^2} - e^{-\beta(K^2 + \omega)}] \\ &= -\frac{m^*\pi}{(2\pi)^2 Q'} \int_{\left(\frac{\omega}{2Q'}\right)^2}^{\infty} dE \frac{1}{\sqrt{E - \left(\frac{\omega}{2Q'}\right)^2}} [e^{-\beta E} - e^{-\beta(E + \omega)}] \\ &\approx -\frac{m^*\omega}{4\pi Q'} \int_{\left(\frac{\omega}{2Q'}\right)^2}^{\infty} dE \frac{\beta e^{-\beta E}}{\sqrt{E - \left(\frac{\omega}{2Q'}\right)^2}} = -\frac{m^*\omega}{4\pi Q'} \sqrt{\beta} \int_{\beta\left(\frac{\omega}{2Q'}\right)^2}^{\infty} dx \frac{e^{-x}}{\sqrt{x - \beta\left(\frac{\omega}{2Q'}\right)^2}} \\ &= -\frac{m^*\omega}{4\pi Q'} \sqrt{\beta} e^{-\beta\left(\frac{\omega}{2Q'}\right)^2} \int_0^{\infty} dx \frac{e^{-x}}{\sqrt{x}} \\ &= -\frac{m^*\omega\sqrt{\beta}}{4\sqrt{\pi}Q'} e^{-\beta\left(\frac{\omega}{2Q'}\right)^2} \end{aligned} \tag{S45}$$

4. Temperature estimate

We estimate the effective temperature of electrons using experimental data on the cooling power provided by phonons. In a Floquet driven system, the effective temperature of the electrons and the temperature of the lattice, which is coupled to a cold bath, can differ. The cooling power is the amount of energy per unit of time that is carried away by the cold lattice (mostly by optical phonons), thus stabilizing the effective electron temperature. While experimental results for the cooling power are available for graphene [94–96], theoretical work [97] shows that the cooling power of TMDs is even larger, leading to a lower effective temperature. Here, for a conservative estimate, we use the values measured for graphene [96], where the lattice was kept at 4.2 K.

The cooling power per electron P strongly depends on the effective temperature of the electrons. In two dimensional materials [97, 98] one finds

$$P_{\text{cool}} = \frac{\Sigma(\bar{\rho})}{\bar{\rho}} (T_e^4 - T_{\text{ph}}^4).$$

This law holds well for electron temperatures below 100 K. T_e is the effective electron temperature, and T_{ph} is the temperature of the lattice. The above assumes that the electrons are thermalized. In fact, one expects a very fast thermalization of the electrons due to electron-electron interactions. For the above estimate of $\bar{\rho} = 1.18 \cdot 10^{11}/\text{cm}^{-2}$, we find $\Sigma(\bar{\rho}) \approx 1 \frac{\text{mW}}{\text{K}^4 \text{m}^2}$. On the other hand, the power supplied by Floquet drive is

$$P_{\text{drive}} \approx \hbar \Omega_F (\Gamma_{\text{int}} + \Gamma_{\gamma}) / \bar{\rho}.$$

Setting $P_{\text{cool}} = P_{\text{drive}}$, we find that cooling and heating rates are balanced at the effective electron temperature

$$T_e \approx 20 \text{ K}. \quad (\text{S } 46)$$

Eq. (S 46) shows that the heating induced by MFPD is not too large. In fact, due to the nonlinear dependence of the cooling power on T_e , the driving power could be easily increased by three orders of magnitude giving a feasible effective temperature of around $T_e \approx 100 \text{ K}$.

Let us finally comment on the Landau damping induced by MFPD. To estimate the factor $e^{-\beta(\frac{\omega}{2q})^2}$ in Eq. (S 45), we assume $T = 300 \text{ K}$ and neglect the small MFPD induced heating. Typically, in experiments, the temperature as well as the Landau damping will be smaller. For a typical plasmon with wavelength $1 \mu\text{m}$ and roughly $\omega = 1 \text{ THz}$, we find

$$\beta \left(\frac{\sqrt{m^*} \omega}{2q} \right)^2 \sim 10^3,$$

such that even at room temperature, the Landau damping is suppressed by a factor of

$$\sim e^{-10^3}.$$

-
- [1] E. Galiffi, R. Tirole, S. Yin, H. Li, S. Vezzoli, P. A. Huidobro, M. G. Silveirinha, R. Sapienza, A. Alù, and J. Pendry, *Photonics of time-varying media*, *Advanced Photonics* **4**, 014002 (2022).
- [2] F. R. Morgenthaler, *Velocity modulation of electromagnetic waves*, *IRE Transactions on microwave theory and techniques* **6**, 167 (1958).
- [3] D. Holberg and K. Kunz, *Parametric properties of fields in a slab of time-varying permittivity*, *IEEE Transactions on Antennas and Propagation* **14**, 183 (1966).
- [4] R. Tirole, E. Galiffi, J. Dranczewski, T. Attavar, B. Tilmann, Y.-T. Wang, P. A. Huidobro, A. Alù, J. B. Pendry, S. A. Maier *et al.*, *Saturable time-varying mirror based on an epsilon-near-zero material*, *Physical Review Applied* **18**, 054067 (2022).
- [5] Y. Peng, *Topological space-time crystal*, *Physical Review Letters* **128**, 186802 (2022).
- [6] Y. Sharabi, A. Dikopoltsev, E. Lustig, Y. Lumer, and M. Segev, *Spatiotemporal photonic crystals*, *Optica* **9**, 585 (2022).
- [7] X. Wang, M. S. Mirmoosa, V. S. Asadchy, C. Rockstuhl, S. Fan, and S. A. Tretyakov, *Metasurface-based realization of photonic time crystals*, *Science Advances* **9**, eadg7541 (2023).
- [8] X. Wang, M. S. Mirmoosa, and S. A. Tretyakov, *Controlling surface waves with temporal discontinuities of metasurfaces*, *Nanophotonics* (2023).
- [9] T. T. Koutserimpas and C. Valagiannopoulos, *Multiharmonic resonances of coupled time-modulated resistive metasurfaces*, *Physical Review Applied* **19**, 064072 (2023).
- [10] A. Akbarzadeh, N. Chamanara, and C. Caloz, *Inverse prism based on temporal discontinuity and spatial dispersion*, *Optics letters* **43**, 3297 (2018).
- [11] V. Pacheco-Peña and N. Engheta, *Temporal aiming*, *Light: Science & Applications* **9**, 129 (2020).
- [12] V. Pacheco-Peña and N. Engheta, *Temporal equivalent of the brewster angle*, *Physical Review B* **104**, 214308 (2021).
- [13] M. Lyubarov, Y. Lumer, A. Dikopoltsev, E. Lustig, Y. Sharabi, and M. Segev, *Amplified emission and lasing in photonic time crystals*, *Science* **377**, 425 (2022).
- [14] J. Mendonça and A. Guerreiro, *Time refraction and the quantum properties of vacuum*, *Physical Review A* **72**, 063805 (2005).
- [15] E. Lustig, Y. Sharabi, and M. Segev, *Topological aspects of photonic time crystals*, *Optica* **5**, 1390 (2018).
- [16] R. Carminati, H. Chen, R. Pierrat, and B. Shapiro, *Universal statistics of waves in a random time-varying medium*, *Physical Review Letters* **127**, 094101 (2021).
- [17] N. Wang, Z.-Q. Zhang, and C. T. Chan, *Photonic floquet media with a complex time-periodic permittivity*, *Physical Review B* **98**, 085142 (2018).
- [18] H. Li, S. Yin, E. Galiffi, and A. Alù, *Temporal parity-time symmetry for extreme energy transformations*, *Physical Review Letters* **127**, 153903 (2021).
- [19] Y. Pan, M.-I. Cohen, and M. Segev, *Superluminal k-gap solitons in photonic time-crystals with kerr nonlinearity*, in *CLEO: QELS_Fundamental Science*, Optica Publishing Group (2022), (FW5J-5).
- [20] V. Bacot, M. Labousse, A. Eddi, M. Fink, and E. Fort, *Time reversal and holography with spacetime transformations*, *Nature Physics* **12**, 972 (2016).
- [21] R. Fleury, A. B. Khanikaev, and A. Alu, *Floquet topological insulators for sound*, *Nature communications* **7**, 11744 (2016).
- [22] X. Wen, X. Zhu, A. Fan, W. Y. Tam, J. Zhu, H. W. Wu, F. Lemoult, M. Fink, and J. Li, *Unidirectional amplification with acoustic non-hermitian space-time varying metamaterial*, *Communications Physics* **5**, 18 (2022).

- [23] T. Oka and H. Aoki, *Photovoltaic hall effect in graphene*, Physical Review B **79**, 081406 (2009).
- [24] T. Kitagawa, T. Oka, A. Brataas, L. Fu, and E. Demler, *Transport properties of nonequilibrium systems under the application of light: Photoinduced quantum hall insulators without landau levels*, Physical Review B **84**, 235108 (2011).
- [25] T. Kitagawa, E. Berg, M. Rudner, and E. Demler, *Topological characterization of periodically driven quantum systems*, Physical Review B **82**, 235114 (2010).
- [26] N. H. Lindner, G. Refael, and V. Galitski, *Floquet topological insulator in semiconductor quantum wells*, Nature Physics **7**, 490 (2011).
- [27] Y. Wang, H. Steinberg, P. Jarillo-Herrero, and N. Gedik, *Observation of Floquet-Bloch states on the surface of a topological insulator*, Science **342**, 453 (2013).
- [28] J. W. McIver, B. Schulte, F.-U. Stein, T. Matsuyama, G. Jotzu, G. Meier, and A. Cavalleri, *Light-induced anomalous hall effect in graphene*, Nature physics **16**, 38 (2020).
- [29] F. Mahmood, C.-K. Chan, Z. Alpichshev, D. Gardner, Y. Lee, P. A. Lee, and N. Gedik, *Selective scattering between Floquet-Bloch and Volkov states in a topological insulator*, Nature Physics **12**, 306 (2016).
- [30] S. Zhou, C. Bao, B. Fan, H. Zhou, Q. Gao, H. Zhong, T. Lin, H. Liu, P. Yu, P. Tang *et al.*, *Pseudospin-selective Floquet band engineering in black phosphorus*, Nature **614**, 75 (2023).
- [31] G. Usaj, P. M. Perez-Piskunow, L. F. Torres, and C. A. Balseiro, *Irradiated graphene as a tunable floquet topological insulator*, Physical Review B **90**, 115423 (2014).
- [32] P. M. Perez-Piskunow, G. Usaj, C. A. Balseiro, and L. F. Torres, *Floquet chiral edge states in graphene*, Physical Review B **89**, 121401 (2014).
- [33] T. Oka and S. Kitamura, *Floquet engineering of quantum materials*, Annual Review of Condensed Matter Physics **10**, 387 (2019).
- [34] O. Katz, G. Refael, and N. H. Lindner, *Optically induced flat bands in twisted bilayer graphene*, Physical Review B **102**, 155123 (2020).
- [35] A. Castro, U. De Giovannini, S. A. Sato, H. Hübener, and A. Rubio, *Floquet engineering the band structure of materials with optimal control theory*, Physical Review Research **4**, 033213 (2022).
- [36] I. Esin, M. S. Rudner, G. Refael, and N. H. Lindner, *Quantized transport and steady states of floquet topological insulators*, Physical Review B **97**, 245401 (2018).
- [37] I. Esin, M. S. Rudner, and N. H. Lindner, *Floquet metal-to-insulator phase transitions in semiconductor nanowires*, Science advances **6**, eaay4922 (2020).
- [38] I. Esin, G. K. Gupta, E. Berg, M. S. Rudner, and N. H. Lindner, *Electronic floquet gyro-liquid crystal*, Nature communications **12**, 1 (2021).
- [39] H. Deghani, T. Oka, and A. Mitra, *Out-of-equilibrium electrons and the hall conductance of a floquet topological insulator*, Physical Review B **91**, 155422 (2015).
- [40] M. Genske and A. Rosch, *Floquet-boltzmann equation for periodically driven fermi systems*, Physical Review A **92**, 062108 (2015).
- [41] L. Glazman, *Kinetics of electrons and holes in direct-gap semiconductors photo-excited by high-intensity pulses*, Soviet Physics Semiconductors-USSR **17**, 494 (1983).
- [42] H. Deghani, T. Oka, and A. Mitra, *Dissipative floquet topological systems*, Physical Review B **90**, 195429 (2014).
- [43] M. Sentef, M. Claassen, A. Kemper, B. Moritz, T. Oka, J. Freericks, and T. Devereaux, *Theory of floquet band formation and local pseudospin textures in pump-probe photoemission of graphene*, Nature communications **6**, 7047 (2015).
- [44] C.-K. Chan, P. A. Lee, K. S. Burch, J. H. Han, and Y. Ran, *When chiral photons meet chiral fermions: photoinduced anomalous hall effects in weyl semimetals*, Physical review letters **116**, 026805 (2016).
- [45] A. Farrell and T. Pereg-Barnea, *Photon-inhibited topological transport in quantum well heterostructures*, Physical Review Letters **115**, 106403 (2015).
- [46] Z. Gu, H. Fertig, D. P. Arovas, and A. Auerbach, *Floquet spectrum and transport through an irradiated graphene ribbon*, Physical review letters **107**, 216601 (2011).
- [47] H. Hübener, M. A. Sentef, U. De Giovannini, A. F. Kemper, and A. Rubio, *Creating stable floquet-weyl semimetals by laser-driving of 3d Dirac materials*, Nature communications **8**, 13940 (2017).
- [48] L. Jiang, T. Kitagawa, J. Alicea, A. Akhmerov, D. Pekker, G. Refael, J. I. Cirac, E. Demler, M. D. Lukin, and P. Zoller, *Majorana fermions in equilibrium and in driven cold-atom quantum wires*, Physical review letters **106**, 220402 (2011).
- [49] D. M. Kennes, N. Müller, M. Pletyukhov, C. Weber, C. Bruder, F. Hassler, J. Klinovaja, D. Loss, and H. Schoeller, *Chiral one-dimensional floquet topological insulators beyond the rotating wave approximation*, Physical Review B **100**, 041103 (2019).
- [50] A. Kundu and B. Seradjeh, *Transport signatures of floquet majorana fermions in driven topological superconductors*, Physical review letters **111**, 136402 (2013).
- [51] M. Thakurathi, D. Loss, and J. Klinovaja, *Floquet majorana fermions and parafermions in driven rashba nanowires*, Physical Review B **95**, 155407 (2017).
- [52] E. I. Kiselev, M. S. Rudner, and N. H. Lindner, *Modulated floquet parametric driving and non-equilibrium crystalline electron states*, arXiv preprint arXiv:2303.02148 (2023).
- [53] S. M. Rezende, A. Azevedo, and R. L. Rodríguez-Suárez, *Introduction to antiferromagnetic magnons*, Journal of Applied Physics **126** (2019).
- [54] A. Kreisel, F. Sauli, L. Bartosch, and P. Kopietz, *Microscopic spin-wave theory for yttrium-iron garnet films*, The European physical journal B **71**, 59 (2009).
- [55] J. Mentink, K. Balzer, and M. Eckstein, *Ultrafast and reversible control of the exchange interaction in Mott insulators*,

Nature communications **6**, 6708 (2015).

- [56] S. Chaudhary, D. Hsieh, and G. Refael, *Orbital floquet engineering of exchange interactions in magnetic materials*, Physical Review B **100**, 220403 (2019).
- [57] A. Ron, S. Chaudhary, G. Zhang, H. Ning, E. Zoghlin, S. Wilson, R. Averitt, G. Refael, and D. Hsieh, *Ultrafast enhancement of ferromagnetic spin exchange induced by ligand-to-metal charge transfer*, Physical Review Letters **125**, 197203 (2020).
- [58] M. B. Lundberg, Y. Gao, R. Asgari, C. Tan, B. Van Duppen, M. Autore, P. Alonso-González, A. Woessner, K. Watanabe, T. Taniguchi, R. Hillenbrand, J. Hone, M. Polini, and F. H. L. Koppens, *Tuning quantum nonlocal effects in graphene plasmonics*, Science **357**, 187 (2017).
- [59] L. D. Landau and E. M. Lifshitz, *Mechanics*, Butterworth-Heinemann (1976). ISBN 978-0750628969.
- [60] L. Turyn, *The damped Mathieu equation*, Quarterly of applied mathematics **51**, 389 (1993).
- [61] J. R. Zurita-Sánchez, P. Halevi, and J. C. Cervantes-Gonzalez, *Reflection and transmission of a wave incident on a slab with a time-periodic dielectric function $\epsilon(t)$* , Physical Review A **79**, 053821 (2009).
- [62] V. Asadchy, A. Lamprianidis, G. Ptitsyn, M. Albooyeh, Rituraj, T. Karamanos, R. Alaee, S. Tretyakov, C. Rockstuhl, and S. Fan, *Parametric mie resonances and directional amplification in time-modulated scatterers*, Physical Review Applied **18**, 054065 (2022).
- [63] H. Rubinsztein-Dunlop, A. Forbes, M. V. Berry, M. R. Dennis, D. L. Andrews, M. Mansuripur, C. Denz, C. Alpmann, P. Banzer, T. Bauer *et al.*, *Roadmap on structured light*, Journal of Optics **19**, 013001 (2016).
- [64] S. Wheaton, R. M. Gelfand, and R. Gordon, *Probing the Raman-active acoustic vibrations of nanoparticles with extraordinary spectral resolution*, Nature Photonics **9**, 68 (2015).
- [65] J. Chen, M. Badioli, P. Alonso-González, S. Thongrattanasiri, F. Huth, J. Osmond, M. Spasenović, A. Centeno, A. Pesquera, P. Godignon, A. Z. Elorza, N. Camara, F. J. García de Abajo, R. Hillenbrand, and F. H. L. Koppens, *Optical nano-imaging of gate-tunable graphene plasmons*, Nature **487**, 77 (2012).
- [66] Z. Fei, A. Rodin, G. O. Andreev, W. Bao, A. McLeod, M. Wagner, L. Zhang, Z. Zhao, M. Thiemens, G. Dominguez, M. M. Fogler, A. H. Castro Neto, C. N. Lau, F. J. Keilmann, and D. N. Basov, *Gate-tuning of graphene plasmons revealed by infrared nano-imaging*, Nature **487**, 82 (2012).
- [67] A. Chaves, J. G. Azadani, H. Alsalman, D. Da Costa, R. Frisenda, A. Chaves, S. H. Song, Y. D. Kim, D. He, J. Zhou *et al.*, *Bandgap engineering of two-dimensional semiconductor materials*, npj 2D Materials and Applications **4**, 1 (2020).
- [68] J. Kim, S. S. Baik, S. H. Ryu, Y. Sohn, S. Park, B.-G. Park, J. Denlinger, Y. Yi, H. J. Choi, and K. S. Kim, *Observation of tunable band gap and anisotropic dirac semimetal state in black phosphorus*, Science **349**, 723 (2015).
- [69] A. Chaves, R. Ribeiro, T. Frederico, and N. Peres, *Excitonic effects in the optical properties of 2d materials: an equation of motion approach*, 2D Materials **4**, 025086 (2017).
- [70] K. I. Seetharam, C.-E. Bardyn, N. H. Lindner, M. S. Rudner, and G. Refael, *Controlled population of Floquet-Bloch states via coupling to Bose and Fermi baths*, Physical Review X **5**, 041050 (2015).
- [71] Note that k_F is fixed by momentum conservation.
- [72] A. A. Abrikosov and I. M. Khalatnikov, *The theory of a fermi liquid (the properties of liquid 3He at low temperatures)*, Reports on Progress in Physics **22**, 329 (1959).
- [73] A. Eguluz and J. Quinn, *Hydrodynamic model for surface plasmons in metals and degenerate semiconductors*, Physical Review B **14**, 1347 (1976).
- [74] D. Forster, *Hydrodynamic Fluctuations, Broken Symmetry, and Correlation Functions*, CRC Press (2018). ISBN 978-0367091323.
- [75] A. Lucas and S. Sachdev, *Memory matrix theory of magnetotransport in strange metals*, Physical Review B **91**, 195122 (2015).
- [76] E. I. Kiselev, *Universal superdiffusive modes in charged two dimensional liquids*, Physical Review B **103**, 235116 (2021).
- [77] D. V. Else, C. Monroe, C. Nayak, and N. Y. Yao, *Discrete time crystals*, Annual Review of Condensed Matter Physics **11**, 467 (2020).
- [78] D. V. Else, B. Bauer, and C. Nayak, *Floquet time crystals*, Physical review letters **117**, 090402 (2016).
- [79] N. Y. Yao, A. C. Potter, I.-D. Potirniche, and A. Vishwanath, *Discrete time crystals: Rigidity, criticality, and realizations*, Physical review letters **118**, 030401 (2017).
- [80] J. Zhang, P. W. Hess, A. Kyprianidis, P. Becker, A. Lee, J. Smith, G. Pagano, I.-D. Potirniche, A. C. Potter, A. Vishwanath *et al.*, *Observation of a discrete time crystal*, Nature **543**, 217 (2017).
- [81] A. Kyprianidis, F. Machado, W. Morong, P. Becker, K. S. Collins, D. V. Else, L. Feng, P. W. Hess, C. Nayak, G. Pagano *et al.*, *Observation of a prethermal discrete time crystal*, Science **372**, 1192 (2021).
- [82] M. Natsheh, A. Gambassi, and A. Mitra, *Critical properties of the prethermal floquet time crystal*, Physical Review B **103**, 224311 (2021).
- [83] N. Y. Yao, C. Nayak, L. Balents, and M. P. Zaletel, *Classical discrete time crystals*, Nature Physics **16**, 438 (2020).
- [84] G. Ni, d. A. McLeod, Z. Sun, L. Wang, L. Xiong, K. Post, S. Sunku, B.-Y. Jiang, J. Hone, C. R. Dean *et al.*, *Fundamental limits to graphene plasmonics*, Nature **557**, 530 (2018).
- [85] E. L. Ince, *Ordinary differential equations*, Courier Corporation (1956).
- [86] The quantity $\epsilon_{\text{pl}}(q)$ is analogous to the quasi-energy of floquet driven electrons.
- [87] C. Gerry, P. Knight, and P. L. Knight, *Introductory quantum optics*, Cambridge university press (2005).
- [88] Z. Sun, D. Basov, and M. Fogler, *Graphene as a source of entangled plasmons*, Physical Review Research **4**, 023208 (2022).
- [89] K. J. Burns, G. M. Vasil, J. S. Oishi, D. Lecoanet, and B. P. Brown, *Dedalus: A flexible framework for numerical simulations with spectral methods*, Physical Review Research **2**, 023068 (2020).
- [90] A. Principi, G. Vignale, M. Carrega, and M. Polini, *Intrinsic lifetime of dirac plasmons in graphene*, Physical Review B

- 88**, 195405 (2013).
- [91] M. S. Rudner and N. H. Lindner, *Band structure engineering and non-equilibrium dynamics in floquet topological insulators*, *Nature reviews physics* **2**, 229 (2020).
- [92] A. Pertsova and A. V. Balatsky, *Excitonic instability in optically pumped three-dimensional Dirac materials*, *Physical Review B* **97**, 075109 (2018).
- [93] S. Sachdev, *Nonzero-temperature transport near fractional quantum hall critical points*, *Physical Review B* **57**, 7157 (1998).
- [94] A. Baker, J. Alexander-Webber, T. Althebaumer, S. McMullan, T. Janssen, A. Tzalenchuk, S. Lara-Avila, S. Kubatkin, R. Yakimova, C.-T. Lin *et al.*, *Energy loss rates of hot Dirac fermions in epitaxial, exfoliated, and cvd graphene*, *Physical Review B* **87**, 045414 (2013).
- [95] A. Baker, J. Alexander-Webber, T. Althebaumer, and R. Nicholas, *Energy relaxation for hot dirac fermions in graphene and breakdown of the quantum hall effect*, *Physical review B* **85**, 115403 (2012).
- [96] A. Betz, F. Vialla, D. Brunel, C. Voisin, M. Picher, A. Cavanna, A. Madouri, G. Fève, J.-M. Berroir, B. Plaçais *et al.*, *Hot electron cooling by acoustic phonons in graphene*, *Physical Review Letters* **109**, 056805 (2012).
- [97] K. Kaasbjerg, K. Bhargavi, and S. Kubakaddi, *Hot-electron cooling by acoustic and optical phonons in monolayers of mos 2 and other transition-metal dichalcogenides*, *Physical Review B* **90**, 165436 (2014).
- [98] S. Kubakaddi, *Interaction of massless Dirac electrons with acoustic phonons in graphene at low temperatures*, *Physical Review B* **79**, 075417 (2009).